

## Resonance effects in simultaneous electron-impact ionization-excitation of helium

Yanghua Fang\* and Klaus Bartschat

*Department of Physics and Astronomy, Drake University, Des Moines, Iowa 50311*

(Received 16 April 2001; published 18 July 2001)

Using a second-order perturbative model for a “fast” incident projectile, together with a convergent  $R$  matrix with pseudostates close-coupling model for the initial bound state and the scattering of a “slow” ejected electron in the field of the ion, we found a substantial effect of autoionizing resonances in simultaneous ionization-excitation of the  $n=2$  states in  $\text{He}^+$ . Although widely ignored to date, we show that the effect must be accounted for in a meaningful comparison between theoretical predictions and the available experimental data.

DOI: 10.1103/PhysRevA.64.020701

PACS number(s): 34.80.Dp

As a highly correlated process, simultaneous electron-impact ionization-excitation, particularly in the presence of autoionizing resonances, represents a major challenge to both experimentalists and theorists. With the rapid advance of computational power, it has recently become possible [1,2] to include both first-order and second-order effects in the interaction of a “fast” projectile with the target, combined with a convergent close-coupling-type description of the initial bound state and the interaction between a “slow” ejected electron and the residual ion.

Treating the ionization-excitation process by a combination of perturbative and nonperturbative methods was also described by Marchalant *et al.* [3], who first used a three-state close-coupling expansion and later refined their method [4] to include a convergent expansion in the evaluation of the first-order term only. In our recent study [1] of simultaneous ionization-excitation processes, however, we noticed that the inclusion of a convergent description for the ejected-electron-residual-ion interaction is important not only for the first-order term, but also for the second-order contribution to the scattering amplitude. Furthermore, resonance effects in the ejected-electron-residual-ion interaction can be important as well and, therefore, energy and angular resolution may play a significant role in comparing experimental data and theoretical predictions for ejected-electron energies in the resonance region [2].

Although the  $(2\ell'2\ell')$  resonances below the threshold for ionization with excitation to the  $2s$  state and the  $2p$  state of  $\text{He}^+$  were studied experimentally about a decade ago by Lower and Weigold [5], McDonald and Crowe [6], and Crowe and McDonald [7], the possible effect of higher-lying resonances has been completely ignored to date in all published comparisons of theoretical predictions and experimental data for the simultaneous ionization-excitation process. An analysis of the  $\text{He}^+$  spectrum, on the other hand, reveals that such resonances might have a major effect for three of the experimentally chosen kinematical situations in the work of Dupré *et al.* [8], Avaldi *et al.* [9], and Rouvellou *et al.* [10], namely those with nominal slow-electron energies of 10 eV and 9.25 eV, respectively. In the ionization-excitation

channel to the  $n=2$  final states of  $\text{He}^+$ , these energies lie between the  $n=3$  and  $n=4$  thresholds, i.e., one can expect a wealth of autoionizing resonances, particularly of the form  $(4\ell'n\ell')$ , to partly decay into the  $n=2$  final ionic states. In the corresponding photoionization problem, these resonances were studied by Menzel *et al.* [11]. In the present project, we therefore investigated the effect of such resonances for the kinematical situations mentioned above.

The principal ideas of our method were outlined in detail by Fang and Bartschat [1] and will not be repeated here. Furthermore, the similarities and the differences between our method and that of Marchalant *et al.* [3,4] were discussed in Fang and Bartschat [2]. Very briefly, we describe a fast ionizing projectile with incident momentum  $\mathbf{k}_0$  by a plane wave and obtain the ionization amplitude for two outgoing electrons with momenta  $\mathbf{k}_1$  and  $\mathbf{k}_2$ , respectively, as

$$f(\mathbf{k}_2, \mathbf{k}_1, \mathbf{k}_0) = f^{B1}(\mathbf{k}_2, \mathbf{k}_1, \mathbf{k}_0) + f^{B2}(\mathbf{k}_2, \mathbf{k}_1, \mathbf{k}_0), \quad (1)$$

where  $f^{B1}$  and  $f^{B2}$  are the first-order and second-order contributions to the scattering amplitude. We use the same close-coupling expansion to represent the initial target state  $|\psi_0\rangle$  and the continuum state  $|\Psi_f^-(\mathbf{k}_2)\rangle$  describing the slow ejected electron in the field of the residual ion, and hence we expect similar convergence properties for both terms. This seems advisable, since the principal effect of the second-order term in the calculation of observable quantities often comes through interference with the first-order amplitude in the bilinear product of scattering amplitudes.

The most important change made in the present work compared to earlier calculations involving the  $R$  matrix with pseudostates (RMPS) expansion for the initial bound state and the ejected-electron-residual-ion interaction [12,1,2] lies in the choice of the  $\text{He}^+$  states included in the close-coupling expansion. As before, we used a 23-state model including ten bound states and 13 continuum pseudostates, with the latter chosen to represent the effect of coupling to the (double) ionization continuum. However, to allow for the proper treatment of autoionizing resonances with configuration  $(4\ell'n\ell')$ , it was necessary to choose *all* the bound states of  $\text{He}^+$  to be physical states, in contrast to the previous work where the  $n=4$  states were chosen as pseudostates to simulate the coupling to the remaining members of the bound spectrum. Note that this choice is likely to not only change

\*Also at Institute for Nuclear Physics, Moscow State University, 119899 Moscow, Russia.

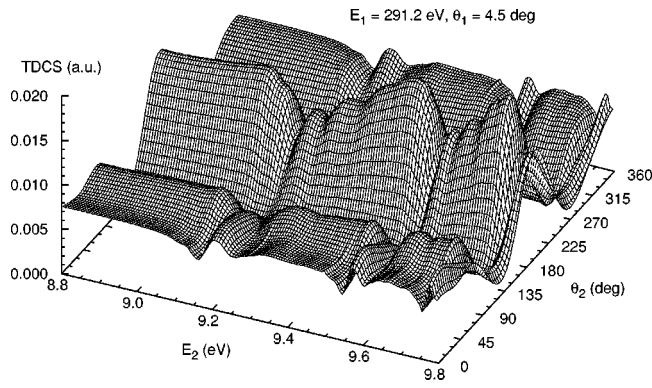


FIG. 1. Ejected-electron energy and angle dependence of the triple-differential cross section, in atomic units  $a_0^2/(2 \text{ Ry sr}^2)$ , for simultaneous ionization-excitation of He  $(1s^2)^1S$  to the  $n=2$  ( $2s+2p$ ) states of He $^+$ . For an incident projectile energy of 365.8 eV and an observation angle of  $\theta_1=4.5^\circ$  for the fast, outgoing electron of energy  $E_1 \approx 291.2$  eV, the PWB2-RMPS results are plotted as a function of the detection angle  $\theta_2$  for slow-electron energies between 8.8 eV and 9.8 eV.

the previous results for slow-electron energies in the vicinity of these resonances. In fact, the amount of the change far away from the resonances will provide an indication about the overall convergence of the close-coupling expansion. In the present study, we found these changes to be sufficiently small to conclude that the principal findings about the possible effects of the  $(4/n\ell')$  resonances on the results presented below are valid — without the need for performing even larger calculations beyond our currently available computational resources.

Figures 1–3 show results for the ejected-electron energy and angle dependence of the triple-differential cross section for simultaneous ionization-excitation of He  $(1s^2)^1S$  to the  $n=2$  ( $2s+2p$ ) states of He $^+$ . These results were obtained in the PWB2-RMPS model mentioned above, i.e., the interaction of the fast projectile with the target was described by a plane-wave Born approximation in first and (approximate) second order, while the initial target state and the interaction

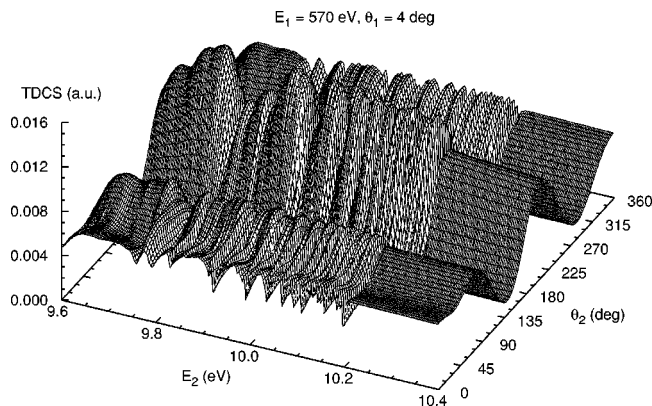


FIG. 2. Same as Fig. 1 for an incident projectile energy of approximately 645 eV and an observation angle of  $\theta_1=4^\circ$  for the fast, outgoing electron of energy  $E_1 \approx 570$  eV. The slow-electron energies range between 9.6 eV and 10.4 eV.

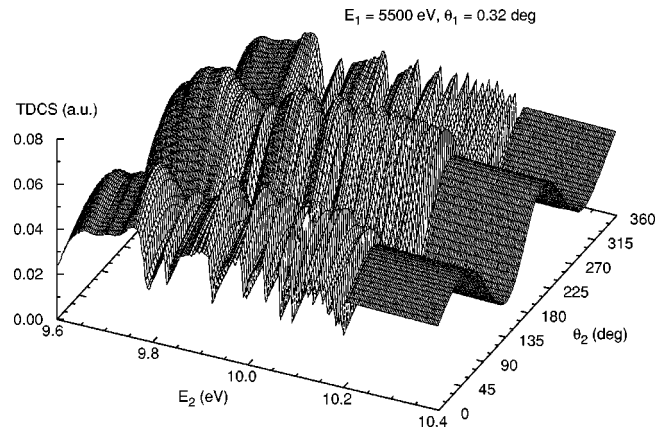


FIG. 3. Same as Fig. 1 for an incident projectile energy of approximately 5575 eV and an observation angle of  $\theta_1=0.32^\circ$  for the fast, outgoing electron of energy  $E_1 \approx 5500$  eV. The slow-electron energies range between 9.6 eV and 10.4 eV.

of the slow ejected electron and the residual ion was described by an RMPS expansion. For the experimentally chosen (energy, angle) combinations for the fast electron of (291.2 eV,  $4.5^\circ$ ) [10], (570 eV,  $4^\circ$ ) [9], and (5500 eV,  $0.32^\circ$ )

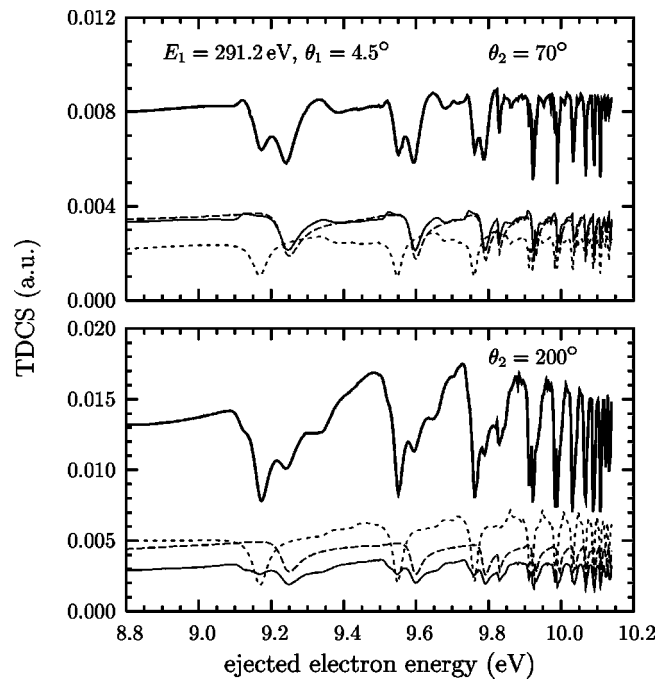


FIG. 4. Ejected-electron energy dependence of the triple-differential cross section for simultaneous ionization-excitation of He  $(1s^2)^1S$  to the  $n=2$  ( $2s+2p$ ) states of He $^+$ . For an incident projectile energy of 365.8 eV and an observation angle of  $\theta_1=4.5^\circ$  for the fast, outgoing electron of energy  $E_1 \approx 291.2$  eV, the PWB2-RMPS results are plotted for ejection angles of  $70^\circ$  and  $200^\circ$  for slow-electron energies between 8.8 eV and 10.2 eV. The thick and thin solid lines represent the PWB2-RMPS and PWB1-RMPS results, respectively, while the long-dashed and short-dashed lines indicate the contributions resulting from total (slow electron plus residual ion) orbital angular momenta  $L=1$  and  $L=2$ , respectively.

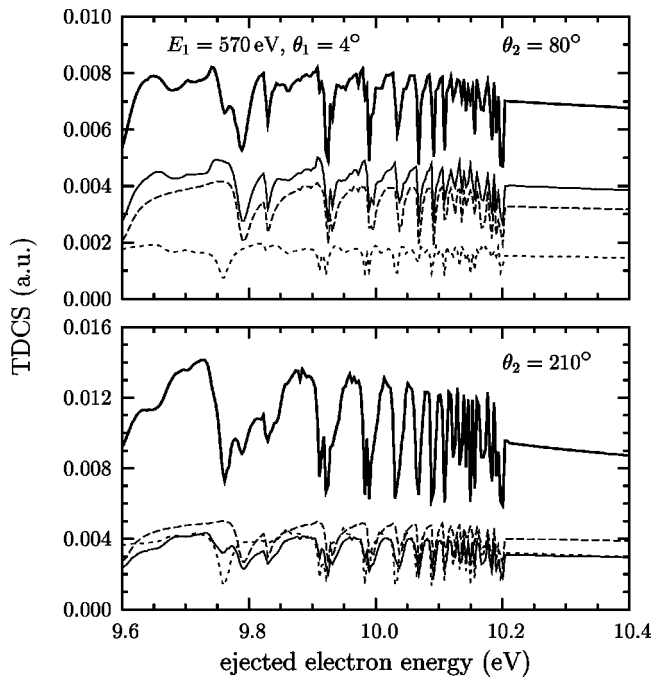


FIG. 5. Same as Fig. 4 for an incident projectile energy of approximately 645 eV and an observation angle of  $\theta_1 = 4^\circ$  for the fast, outgoing electron of energy  $E_1 \approx 570$  eV. The slow-electron energies range between 9.6 eV and 10.4 eV.

[8], the results are plotted in the vicinity of the nominal slow-electron energies of 9.25 eV and 10 eV, respectively. As can be seen from the figures, the potential effect of resonances in an experiment with finite-energy resolution should certainly not be ignored.

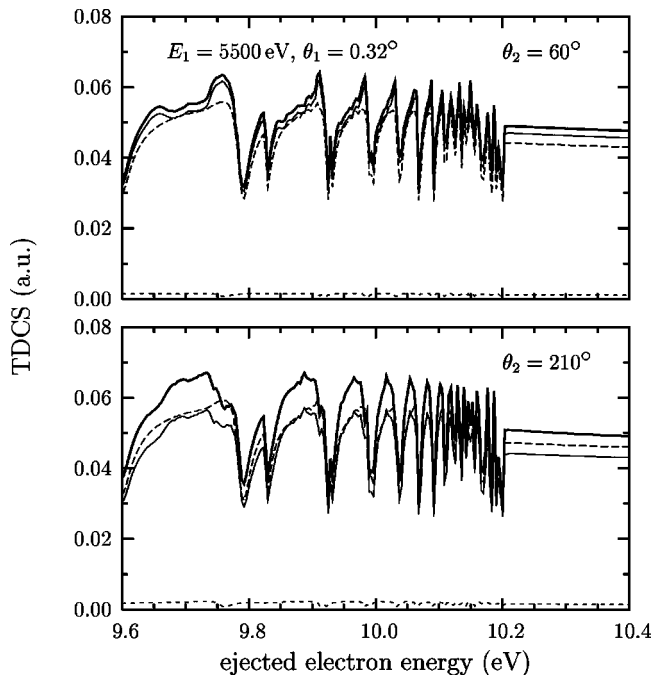


FIG. 6. Same as Fig. 4 for an incident projectile energy of approximately 5575 eV and an observation angle of  $\theta_1 = 4^\circ$  for the fast, outgoing electron of energy  $E_1 \approx 5500$  eV. The slow-electron energies range between 9.6 eV and 10.4 eV.

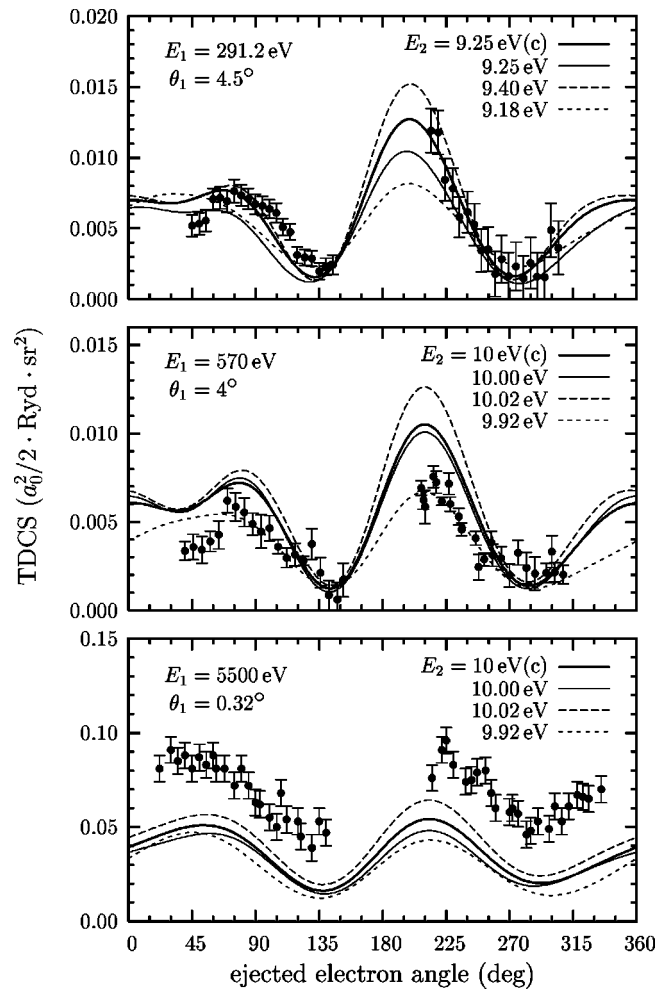


FIG. 7. Ejected-electron angle dependence of the triple-differential cross section for simultaneous ionization-excitation of He ( $1s^2$ ) $^1S$  to the  $n=2$  ( $2s+2p$ ) states of He $^+$ . For fast-electron (energy, angle) combinations of (291.2 eV,  $4.5^\circ$ ), (570 eV,  $4^\circ$ ), and (5500 eV,  $0.32^\circ$ ), the PWB2-RMPS results are plotted for slow-electron energies around 9.25 eV and 10 eV, respectively. To illustrate the effect of a finite-energy resolution, the results marked (c) were convoluted with a Gaussian profile of width 400 meV (FWHM), while the other curves are for the energies given in the legend. The experimental data are taken from Rouvellou *et al.* [10] (top, normalized to the PWB2-RMPS), Avaldi *et al.* [9] (center), and Dupré *et al.* [8] (bottom).

To illustrate this point further, Figs. 4–6 present the ejected-electron energy dependence of the triple-differential cross section in the above kinematical situations, this time for two fixed slow-electron detection angles near the predicted maxima corresponding to the binary and recoil peaks. In addition to the PWB2-RMPS, results summed to convergence over the partial-wave angular momentum of the ejected electron, we also show the first-order PWB1-RMPS results and the contributions from the dipole ( $\lambda=1$ ) and quadrupole ( $\lambda=2$ ) terms in the projectile-target interaction. The latter two are the dominant contributions for relatively low incident projectile energies, while the high-energy case (Fig. 6) is completely dominated by the dipole term in the projectile-target interaction, resulting in relatively small second-order

effects and predominantly a total (slow electron plus residual ion) orbital angular momentum  $L=1$ .

Finally, Fig. 7 shows comparisons of the PWB2-RMPS predictions with the available experimental data in the above cases. We see that a small change in the theoretical energy chosen for comparison can have significant effects on both the shape and the magnitude of the predictions. Also, we note that the angular dependence from the calculation at the nominal ejected energy of 9.25 eV at the top of the figure is quite different from what we obtain after convoluting with a typical Gaussian energy profile of 400 meV (FWHM). (The actual energy resolution in the Dupré *et al.* [8] experiment was 5 eV, indicating that even their results at a nominal slow-electron energy of 5 eV could be affected by resonances, particularly those associated with the  $n=3$  threshold. A realistic calculation for such an energy width would require a number of theoretical points beyond our current computational resources.) Interestingly, our results after convolution are very similar in shape, but different in magnitude, from those obtained for the nominal energy of 9.25 eV in the most recent calculation by Marchalant *et al.* [13]. Note, however, that these particular experimental data are not absolute and have been normalized to provide a good visual fit to the theoretical predictions after convolution.

The convoluted results and those for slow-electron energies of 10 eV are — coincidentally in light of the dense resonance structure — very similar in the other two cases. Consequently, there is no substantial improvement in the agreement between theory and the (absolute) experimental data in the magnitude of the results. As before, the agreement in shape is excellent and certainly has not deteriorated through the convolution procedure. Since changing the theoretical energy by just 100 meV can change the magnitude of the predictions by a factor of 2, however, it seems clear that direct comparisons without convolution could be very misleading.

In summary, we have presented detailed results from a second-order calculation for electron-impact ionization excitation of helium for the energy region near the  $(4\ell/n\ell')$  resonances in the ejected-electron–residual-ion channel. The overall agreement with the existing experimental data is improved when the effect of these autoionizing resonances is properly accounted for. Furthermore, previously made direct comparisons between the available experimental data and calculations for the nominal energy of the slow electron should be revised for the cases discussed here.

This work was supported by the United States National Science Foundation under Grant No. PHY-0088917.

- 
- [1] Y. Fang and K. Bartschat, *J. Phys. B* **34**, L19 (2001).
  - [2] Y. Fang and K. Bartschat, *J. Phys. B* **34**, 2747 (2001).
  - [3] P.J. Marchalant, C.T. Whelan, and H.R.J. Walters, *J. Phys. B* **31**, 1141 (1998).
  - [4] P.J. Marchalant, J. Rasch, C.T. Whelan, D.H. Madison, and H.R.J. Walters, *J. Phys. B* **32**, L705 (1999).
  - [5] J. Lower and E. Weigold, *J. Phys. B* **23**, 2819 (1990).
  - [6] D.G. McDonald and A. Crowe, *Z. Phys. D: At., Mol. Clusters* **23**, 371 (1992).
  - [7] A. Crowe and D.G. McDonald, in *(e,2e) and Related Processes*, edited by C.T. Whelan, H.R.J. Walters, A. Lahmam-Bennani, and H. Ehrhardt (Kluwer, Dordrecht, 1993), pp. 383–392.
  - [8] C. Dupré, A. Lahmam-Bennani, A. Duguet, F. Mota-Furtado, P.F. O'Mahony, and C.D. Capello, *J. Phys. B* **25**, 259 (1992).
  - [9] L. Avaldi, R. Camilloni, R. Multari, G. Stefani, O. Robaux, R.J. Tweed, and G.N. Vien, *J. Phys. B* **31**, 2981 (1998).
  - [10] B. Rouvellou, S. Rioual, A. Pochat, R.J. Tweed, J. Langlois, G.N. Vien, and O. Robaux, *J. Phys. B* **33**, L599 (2000).
  - [11] A. Menzel, S.P. Frigo, S.B. Whitfield, C.D. Caldwell, and M.O. Krause, *Phys. Rev. A* **54**, 2080 (1996).
  - [12] A.S. Kheifets, I. Bray, and K. Bartschat, *J. Phys. B* **32**, L433 (1999).
  - [13] P.J. Marchalant, B. Rouvellou, J. Rasch, S. Rioual, C.T. Whelan, A. Pochat, D.H. Madison, and H.R.J. Walters, *J. Phys. B* **33**, L749 (2000).